energies

MDPI

Article

A Non-Empirical Fractal Permeability Model for EOR in Hydrate-Bearing Reservoirs: Coupling Effects of Effective Stress, Temperature, and Particle Heterogeneity

Ying-Ying Ma [1,2], Yi-Han Shang [1,2], Ke-Yi Wang [1,2] and Gang Lei [1,2,*]

[1] National Center for International Research on Deep Earth Drilling and Resource Development, Faculty of Engineering, China University of Geosciences, Wuhan 430074, China; myy0325@163.com (Y.-Y.M.); shangyh@cug.edu.cn (Y.-H.S.); kellywango@cug.edu.cn (K.-Y.W.)
[2] Institute for Advanced Marine Research, China University of Geosciences, Guangzhou 511462, China
* Correspondence: leigang@cug.edu.cn

Abstract

Permeability is a critical parameter for evaluating the production potential of natural gas hydrate reservoirs, and its accurate prediction is essential for enhanced oil recovery (EOR). However, existing permeability models often assume a uniform particle distribution, neglecting the inherent heterogeneity of natural sediments, and rarely fully couple the effects of effective stress and temperature variations induced by EOR operations. To address that gap, this study develops a novel non-empirical fractal permeability model that incorporates particle heterogeneity through an offset angle (θ) and an aspect ratio (m), and couples these with thermoelastic theory to describe the evolution of the pore structure under coupled thermo-mechanical conditions. The model accounts for two hydrate growth habits (grain-coating and pore-filling) and allows for their coexistence via weighting coefficients. Using this model, we systematically investigate the individual and combined effects of effective stress, temperature, particle heterogeneity, and hydrate saturation on permeability. Model predictions are validated against independent experimental data from multiple sources, showing good agreement. The results reveal that permeability decreases with increasing effective stress and temperature, with stress playing a more dominant role; moreover, the transition between hydrate growth habits under stress is captured. The proposed model provides a theoretical tool to understand permeability evolution in heterogeneous hydrate reservoirs under varying thermo-mechanical conditions, thereby supporting EOR strategy optimization.

Keywords: hydrate-bearing sediments; permeability; effective stress; temperature; particle heterogeneity; EOR

Check for updates

Academic Editor: Hossein Hamidi

Received: 7 February 2026
Revised: 23 February 2026
Accepted: 27 February 2026
Published: 3 March 2026

Copyright: © 2026 by the authors. Licensee MDPI, Basel, Switzerland. This article is an open access article distributed under the terms and conditions of the Creative Commons Attribution (CC BY) license.

1. Introduction

Natural gas, a clean and abundantly available energy source, plays a pivotal role in satisfying the global energy demand and tackling environmental challenges [1]. As an important form of natural gas occurrence, natural gas hydrates (NGHs) are extensively distributed in permafrost zones and deep-sea sediments, and they are recognized as a highly promising energy resource for the future [2]. Currently, the commercial development of hydrates primarily involves exploration, extraction, and transportation [3–5]. Mainstream extraction technologies include depressurization, thermal stimulation, chemical injection, and the CO_2 replacement method [6,7]. Among these, chemical injection techniques—such

as acid stimulation—have been extensively studied in conventional reservoirs to enhance permeability by dissolving minerals and creating flow channels, as demonstrated in carbonate rocks by Jia et al. [8]. However, regardless of the method employed, permeability remains one of the most critical physical parameters for evaluating the gas production potential of a reservoir and optimizing extraction schemes [9], which is crucial for evaluating and predicting the production and recoverable reserves of natural gas hydrate resources [10]. Recent advances in mathematical modeling, such as the application of machine learning techniques for production rate forecasting in complex fields [11], further underscore the need for accurate input parameters like permeability to improve prediction reliability. Accurate evaluation of reservoir permeability is crucial for predicting gas production profiles, optimizing well placement, and assessing the economic feasibility of long-term exploitation. However, natural gas hydrate reservoirs are usually located in complex geological settings of deepwater or permafrost regions. Their permeability is strongly influenced by the inherent heterogeneity of sediments, hydrate saturation and occurrence habits, as well as dynamically changing external conditions (e.g., effective stress and temperature) during exploitation. Traditional permeability models often fail to comprehensively capture the synergistic effects of these coupled factors, leading to considerable uncertainty in prediction results. Permeability can not only assess the development potential and value of reservoirs but also directly affects NGH extraction efficiency and the selection of extraction methods [12].

The permeability determines the seepage ability of sediments due to the coupled effects of various factors, such as pore structure [13], grain size [14], matric composition [15], effective stress [16,17], temperature and others [18]. In addition, the saturation, distribution and growth mode of hydrates also have certain influences on permeability [19]. However, accurately predicting the permeability of hydrate sediment has always been a hot and challenging issue [20]. For example, scholars (Bernabe et al. [21], Wang et al. [22], and Singh et al. [23]) derived permeability models to reveal the effects of pore structures on permeability in hydrate sediments. Cheng et al. [24], Sun et al. [25] and Song et al. [26] investigated the coupled effects of effective stress and temperature on the permeability of hydrate sediments, respectively. However, current prediction models often assume a uniform distribution of sediment particles, ignoring the heterogeneity of sediments. Recently, Shang et al. [27] derived a theoretical permeability model for HBS considering a heterogeneous particle distribution, effective stress, hydrate saturation and hydrate pore morphology. However, in that work, stress-dependent porosity was determined by a creep constitutive model, and the evolution of a heterogeneous particle distribution under stress and temperature was not explicitly addressed. In contrast, the present model employs thermoelastic theory to directly derive the evolution of particle arrangement parameters (θ and m) under coupled stress and temperature conditions, thereby providing a more mechanistic description of permeability changes during EOR operations. Thus, in this work, we will derive a new permeability model and reveal the evolution of a heterogeneous particle distribution during the change in effective stress and temperature. Furthermore, few models successfully integrate the combined effects of heterogeneity, effective stress, and temperature, leading to deviations between predicted results and actual conditions.

Leveraging the findings of prior research, we conduct a comprehensive analysis of how particle heterogeneity, temperature, and effective stress influence permeability in this study. And we establish a new non-empirical fractal model for calculating permeability, aiming to deepen our understanding of natural gas hydrate reservoirs and improve the accuracy of gas extraction and production predictions. Then, we compare and validate the model using experimental data from other researchers, demonstrating the accuracy and

practicality of the model. Finally, we use numerical simulations to investigate how each parameter affects permeability.

2. Modeling

2.1. Model Assumptions

Building on the assumption of grain coating (GC) hydrates and pore filling (PF) hydrates within the reservoir, a permeability model is derived in this work [28]. We characterize the heterogeneity of sediment using the offset angle θ and heterogeneity parameter m [29]. Here, the offset angle θ quantifies the deviation of the particle alignment from the direction of fluid flow, reflecting the geometric arrangement of particles. The aspect ratio m (defined as the ratio of center-to-center distances, c/b, normal to and along the flow direction) characterizes the elongation or compression of the pore space. Together, these two parameters provide a quantitative description of the sediment's microstructural heterogeneity. Additionally, we assume that the elastic deformation of sediment particles follows Hooke's law. We also assume that solid particles undergo linear expansion when heated.

2.2. Theoretical Model

During the extraction of natural gas hydrates, changes in temperature and effective stress directly cause the deformation of particles and pores, thereby altering pore structure parameters. Based on the thermoelastic theory, assuming that sediment particles undergo linear thermal expansion under temperature changes and elastic deformation following Hooke's law under effective stress, the changes in pore volume due to temperature and stress variations can be derived separately. This leads to an expression for porosity under coupled temperature–pressure conditions. Specifically, this expression can be used to update the porosity value after deformation, providing a foundation for subsequent permeability calculations. The formula for calculating porosity considering the coupling effects of temperature and pressure is presented below:

$$\varphi = 1 - \left(\frac{1 + \alpha \Delta T}{1 - F/E}\right)^2 (1 - \varphi_0) \tag{1}$$

where φ_0 is the initial porosity of sediments; and the parameters F, ΔT, E and α represent effective stress (MPa), temperature variation (°C), elastic modulus (MPa) and linear expansion coefficient (k^{-1}).

Based on Equation (1), the effective porosity φ_e of the hydrate sediments with hydrate saturation S_h is

$$\varphi_e = 1 - \left(\frac{1 + \alpha \Delta T}{1 - F/E}\right)^2 [1 - \varphi_0(1 - S_h)] \tag{2}$$

where S_h is the hydrate saturation after the change in pore volume.

It is assumed that the volume of hydrates remain the same during the deformation of sediments; thus, hydrate saturation S_h can be determined as follows [30]:

$$S_h = \frac{\varphi_0(1 - \varphi)S_{h0}}{\varphi(1 - \varphi_0)} \tag{3}$$

where S_{h0} is the initial hydrate saturation.

This paper discusses two growth modes of hydrates: grain-cementing hydrates (GC) and pore-filling hydrates (PF) [31]. For the GC hydrates, after changes in effective stress and temperature, the maximum pore diameter are [31]

$$\lambda_{\max,GC} = \lambda_{\max,0,GC}\sqrt{1-S_h}\left[\frac{(2-D_{f,0,GC})(3-D_{f,GC})}{(2-D_{f,GC})(3-D_{f,0,GC})}\right] \tag{4}$$

where $\lambda_{\max,0,GC}$ denotes the initial maximum pore diameter for GC hydrates, and $D_{f,0,GC}$ represents the initial pore fractal dimension for GC hydrates, both of which are independent of effective stress and temperature. In contrast, $D_{f,GC}$ is the pore fractal dimension that incorporates the coupled effects of effective stress and temperature.

Based on the fractal theory [32], the pore fractal dimension of sediments can be characterized by fundamental pore structural parameters. From the relationship between the maximum pore size and the fractal dimension established in Equation (4), and in conjunction with the definition of porosity, the expression for the initial pore fractal dimension $D_{f,0,GC}$, as well as the expression for the fractal dimension under given effective stress and temperature conditions $D_{f,GC}$, can be derived. Furthermore, we considering the influence of pore geometry complexity on transport properties; $D_{f,GC}$ can also be related to the tortuosity fractal dimension $D_{\tau,GC}$, yielding an equivalent expression.

$$\begin{cases} D_{f,0,GC} = 2 - \frac{\ln[\varphi_0(1-S_h)]}{\ln(\lambda_{\min,GC}/\lambda_{\max,GC})} \\ D_{f,GC} = 2 - \frac{\ln \varphi_e}{\ln(\lambda_{\min,GC}/\lambda_{\max,GC})} \end{cases} \tag{5}$$

and

$$D_{\tau,GC} = 1 + \frac{\ln\{[\tau_{avF,T}(D_{f,GC} + D_{\tau,GC} - 1)]/D_{f,GC}\}}{\ln(L/\lambda_{\min,GC})} \tag{6}$$

Taking into account heterogeneity, effective stress and temperature effects, the calculation formula for $\tau_{avF,T}$ can be expressed as follows (detailed derivation can be found in Appendix A):

$$\tau_{avF,T} = \frac{1}{4}\left[\begin{array}{l} \frac{r(\pi-2)(1+\alpha\Delta T)}{b(1-F/E)} + \frac{1}{\cos\theta} \\ +\sqrt{\left[1-2\frac{r(1+\alpha\Delta T)}{b(1-F/E)}\sin\theta\right]^2 + (\tan\theta)^2} \\ +\frac{2r\theta(1+\alpha\Delta T)}{b(1-F/E)} \end{array}\right] + \frac{1}{2} + \frac{r(\pi-2)(1+\alpha\Delta T)}{4b(1-F/E)} \tag{7}$$

where parameters r and θ refer to the particle radius (μm) and the angle between the flow direction and the line connecting the centers of two adjacent particles (°), respectively. Parameters b and c denote the center-to-center distances of two particles along and normal to the flow direction (μm), respectively.

Given that the quotient of the minimum-to-maximum pore radius in HBS is reported to be no greater than 0.01 [33], this study adopts a simplified ratio of 0.01, aligning with the methodologies of Tang et al. [30]. This value is widely adopted in fractal-based studies of porous media. The Representative Elementary Volume (REV) is defined as the smallest volume over which a measurement can be made that yields a value representative of the whole macroscopic porous medium. In this fractal model, the cross-sectional area A_{GC} and

the capillary characteristic length L_{GC} of the REV are determined based on the pore-size distribution and fractal scaling laws, as follows:

$$\begin{cases} A_{GC} = \frac{\pi D_{f,GC} r_{max,GC}^2}{2-D_{f,GC}} \left(\frac{r_{max,GC}^{2-D_{f,GC}}}{r_{min,GC}^{2-D_{f,GC}}} - 1 \right) \\ L_{GC} = \sqrt{A_{GC}} \end{cases} \tag{8}$$

According to the fractal model [29], the permeability of grain coating (GC) hydrates K_{GC} is [34,35]

$$KGC = \frac{\pi}{128} \frac{L_{GC}^{(1-D_{\tau,GC})}}{A_{GC}} \frac{D_{f,GC}}{3+D_{\tau,GC}} (\lambda_{max,GC})^{3+D_{\tau,GC}} \tag{9}$$

For pore-filling hydrates (PF), a similar modeling approach is adopted. Under the combined influence of effective stress and temperature, the maximum pore diameter $\lambda_{max,PF}$ is expressed as [31]

$$\lambda_{maxax,PF} = \lambda_{max,0,PF} \left(1 - \sqrt{S_h}\right) \left[\frac{(2-D_{f,0,PF})(3-D_{f,PF})}{(2-D_{f,PF})(3-D_{f,0,PF})} \right] \tag{10}$$

where $\lambda_{max,0,PF}$ denotes the initial maximum pore diameter for PF hydrates. Correspondingly, the initial pore fractal dimension $D_{f,0,PF}$, and the pore fractal dimension under given effective stress and temperature conditions $D_{f,PF}$, are respectively defined as

$$\begin{cases} D_{f,0,PF} = 2 - \frac{\ln[\varphi_0(1-S_h)]}{\ln(\lambda_{min,PF}/\lambda_{max,PF})} \\ D_{f,PF} = 2 - \frac{\ln \varphi e}{\ln(\lambda_{min,PF}/\lambda_{max,PF})} \end{cases} \tag{11}$$

The tortuosity fractal dimension $D_{\tau,PF}$ is [32]

$$D_{\tau,PF} = 1 + \frac{\ln\{[\tau_{avF,T}(D_{f,PF} + D_{\tau,PF} - 1)]/D_{f,PF}\}}{\ln(L/\lambda_{min,PF})} \tag{12}$$

Once the pore-structure parameters are determined, the cross-sectional area A_{PF} and the characteristic capillary length L_{PF} of the REV are calculated as follows:

$$\begin{cases} A_{PF} = \frac{\pi D_{f,PF} r_{max,PF}^2}{2-D_{f,PF}} \left(\frac{r_{max,PF}^{2-D_{f,PF}}}{r_{min,PF}^{2-D_{f,PF}}} - 1 \right) \\ L_{PF} = \sqrt{A_{PF}} \end{cases} \tag{13}$$

Finally, based on fractal theory, the permeability for the pore-filling hydrate morphology K_{PF} is derived as [34,35]

$$K_{PF} = \frac{\pi}{128} \frac{L_{PF}^{(1-D\tau,PF)}}{A_{PF}} \frac{D_{f,PF}}{3+D_{\tau,PF}} (\lambda_{max,PF})^{3+D_{\tau,PF}} \tag{14}$$

2.3. Workflow of Permeability Determination

Based on the theoretical derivations presented in the preceding section, the HBS permeability can be determined through a systematic, step-by-step procedure without introducing any empirical fitting parameters. First, the required input parameters are specified, including the initial porosity φ_0, initial hydrate saturation S_{h0}, initial maximum pore diameter $\lambda_{max,0}$, minimum pore diameter $\lambda_{min,0}$, as well as the particle heterogeneity parameter m and offset angle θ. In addition, the effective stress and temperature conditions acting on the sediment are defined.

Under the prescribed stress and temperature conditions, the porosity of the sediment after deformation, φ, is first calculated using Equations (1) and (2), which account for pore volume variations induced by mechanical compression and thermal expansion. Subsequently, the updated hydrate saturation S_h is determined from Equation (3).

The evolution of the pore structure is then evaluated. The maximum pore diameter λ_{max} under effective stress is obtained from Equation (4), while the pore fractal dimension D_f is calculated using Equation (5) based on the updated porosity and hydrate saturation. The average tortuosity $\tau_{avF,T}$ and the tortuosity fractal dimension D_τ are then determined using Equations (7) and (6), which explicitly incorporate the effects of particle heterogeneity through the parameters m and θ.

Subsequently, the geometric characteristics of the REV are evaluated. A and L are calculated using Equation (8), providing the required geometric input for the capillary bundle representation of the pore structure.

Finally, the permeability of sediments is calculated. The permeability corresponding to the grain-coating hydrate morphology, K_{GC}, is obtained from Equation (9), whereas the permeability associated with the pore-filling hydrate morphology, K_{PF}, is calculated using Equation (14). Since HBS generally exhibits a coexistence of different hydrate occurrence modes, weighting coefficients λ_1 and λ_2 are introduced to determine the permeability as $K = \lambda_1 K_{GC} + \lambda_2 K_{PF}$.

3. Results and Discussion

3.1. Model Validation

Initially, the influence of effective stress variations on permeability under isothermal conditions is validated. Figure 1 presents a comparison between the model predictions and the experimental measurements reported by Zhang et al. [34,35]. Using clay-silty core samples retrieved from the Shenhu hydrate region in the South China Sea as the skeletal framework, Zhang et al. [35] prepared tetrahydrofuran hydrate-bearing sediments with hydrate saturations ranging from 0 to 0.6. They used a custom-designed permeability measurement system to measure the corresponding permeability values under different effective stresses. An initial porosity of 0.55 was utilized in the experiments, and the grain size of the tested cores was observed to span 0.5 to 100 μm. Accordingly, to align the model's initial conditions (porosity and permeability) with the experimental data, the following key parameters are adopted in our model: ψ_0 = 0.55, $r_{max,0}$ = 4.7 μm, E_0 is set to 30 MPa, and b is set to 100 MPa. The upper and lower curves in Figure 1 represent the predicted permeability for grain-coating (GC) and pore-filling (PF) hydrate morphologies, respectively. From Figure 1, it is evident that our predicted data is in basic agreement with the experimental data. The top and bottom curves in the graph represent the predicted permeability curves of GC hydrate and PF hydrate, respectively. Since real reservoirs typically contain a mixture of hydrate types rather than just one, introducing a weighting parameter λ_1 and λ_2 can reflect the proportion and transformation of the two hydrate modes in the reservoir. Additionally, it can be seen that initially the hydrates are mainly in the GC mode, gradually transitioning to predominantly the PF mode with an increase in effective stress; the results from the graph also show that when the initial hydrate saturation is constant, the permeability decreases with an increase in effective stress, and the decreasing trend becomes increasingly gradual. The main reason for this is the compression of pores due to effective stress.

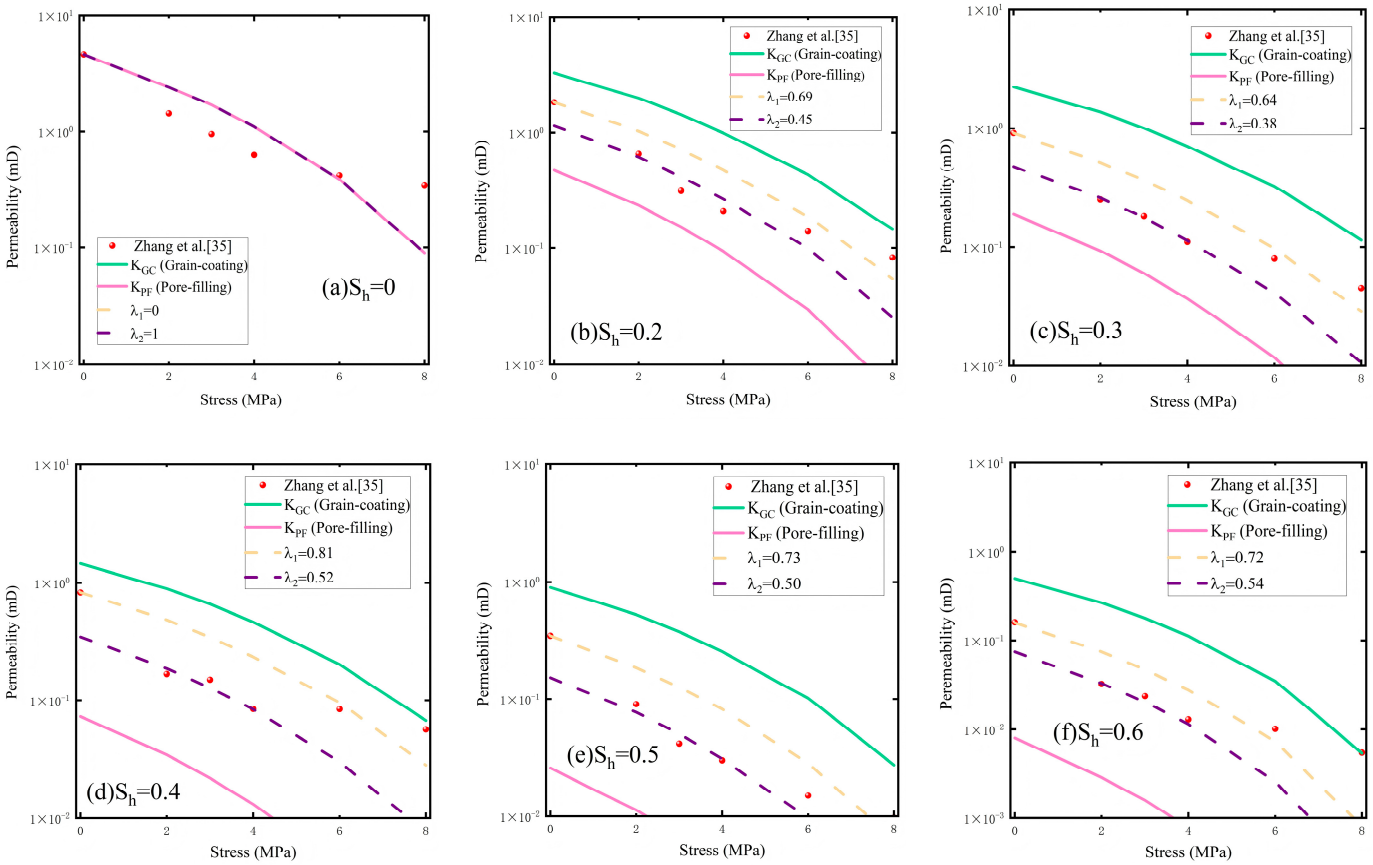


Figure 1. Validation of model permeability predictions with experimental results.

Figure 2 compares the predicted permeability with the experimental data from Cheng et al. [24]. Cheng et al. [24] performed a suite of experiments to quantify the evolution of effective permeability in hydrate-bearing sediments with varying hydrate saturation, under effective stresses ranging from 1 to 9 MPa. The quartz sands were utilized to mimic soil serving as host sediments for the formation of HBS, where an initial porosity of 41.1%, an initial pore pressure of 6 MPa, and a temperature of 274.15 K were applied. For the purpose of matching the predicted results and the experimental data, φ_0 = 0.411, $r_{max,0}$ = 40 μm, $r_{min,0}$ = 0.1 μm, E_0 is set to 180 MPa, and b is set to 400 MPa. The results from the figure show that the values predicted by the model fit well with the experimental data, and in this experiment, the hydrate mode was mainly GC. The permeability shows a decreasing trend with increasing effective stress, which is consistent with expectations.

Then, we validate the effect of temperature variation on permeability at a certain effective stress. Figure 3 compares the predicted permeability with the experimental data from Sun et al. [25]. Sun et al. [25] conducted experiments to measure the change in permeability with increasing temperature (25–95 °C) at different levels of effective stress (2−42 MPa), and the results show that the permeability declines with increasing temperature from 25 °C to 65 °C, but rises as the temperature is elevated from 80 °C to 95 °C. The main reason for the increase in permeability when the temperature exceeds 65 °C is the generation of thermal cracks. Since this point is not considered in our model, we only validate the effect of temperature variation from 25 °C to 65 °C on permeability under effective stress conditions ranging from 2 MPa to 12 MPa. From the results in the figure, it can be observed that at low temperatures, the permeability shows a linear decreasing trend with increasing temperature, and our model closely matches the experimental results.

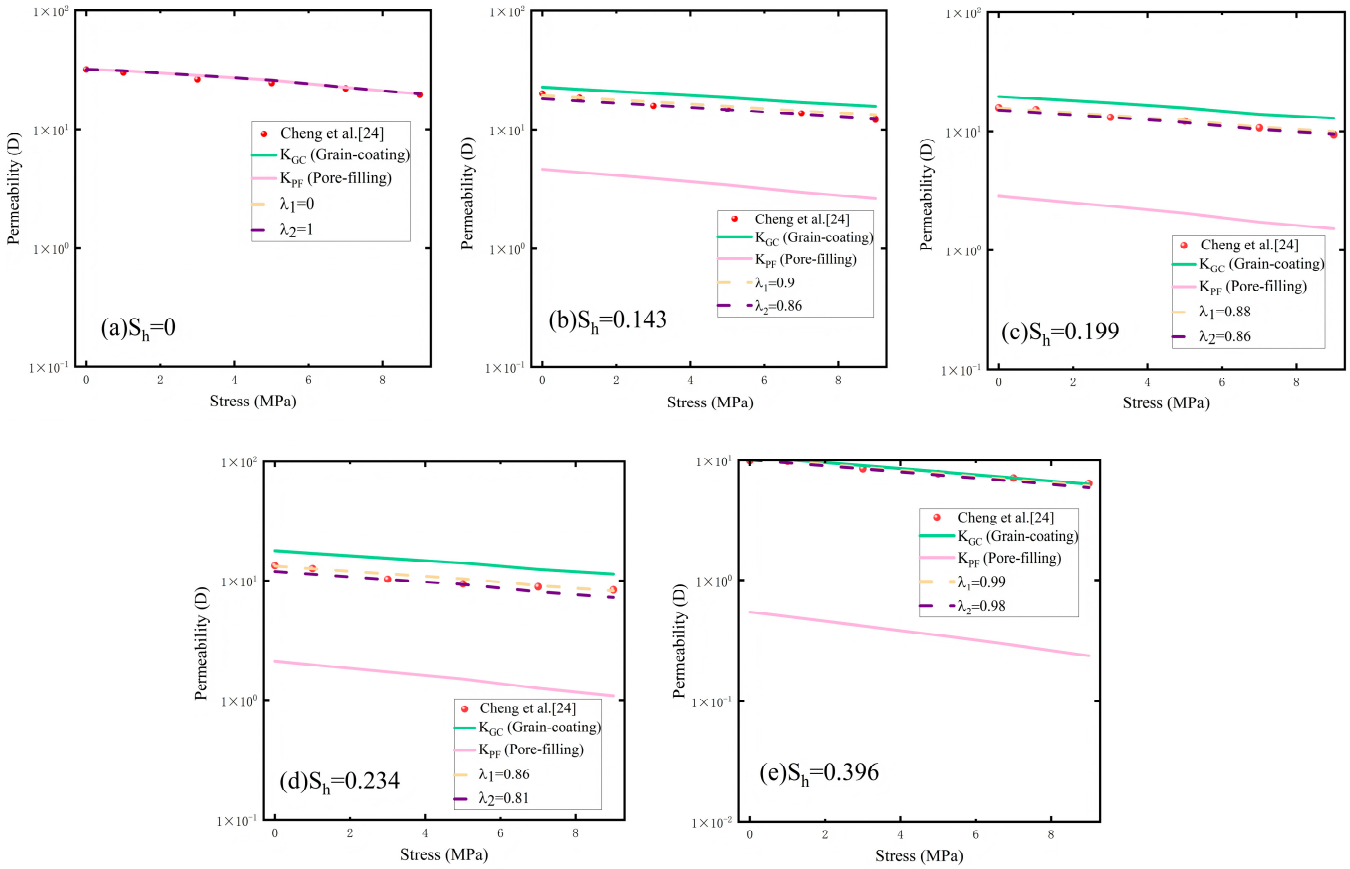


Figure 2. Comparison of model outputs with laboratory measurements.

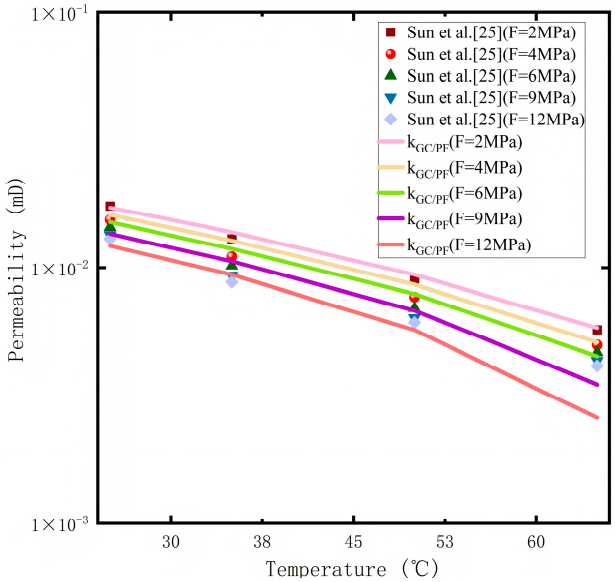


Figure 3. Comparison of predicted permeability with experimental data.

3.2. Sensitivity Analysis

Figure 4a shows that under a constant effective stress condition, the lower the elastic modulus, the greater the decrease in permeability, and the higher the elastic modulus, the smaller the decrease. Figure 4b shows that under constant effective stress conditions, the lower the initial porosity, the greater the decrease in permeability, and when the initial porosity is fixed, the rate of decrease in permeability gradually slows down with increasing effective stress. Figure 4c shows that the higher the initial hydrate saturation,

the lower the initial permeability; when the initial hydrate saturation is 0, the permeability of the sediment is the highest, and the magnitude of decrease with increasing stress is also the highest. Figure 4d indicates that the greater the increase in the linear expansion coefficient, the larger the magnitude of decrease in permeability. However, in terms of the numerical value of permeability, the impact of changes in the linear expansion coefficient on permeability is not significant, as its magnitude is small, at 10^{-6}. Figure 4e illustrates the combined effects of effective stress and temperature variations on permeability. Increasing effective stress and temperature both lead to a decrease in permeability. However, the impact of temperature on permeability is not as great as that of effective stress.

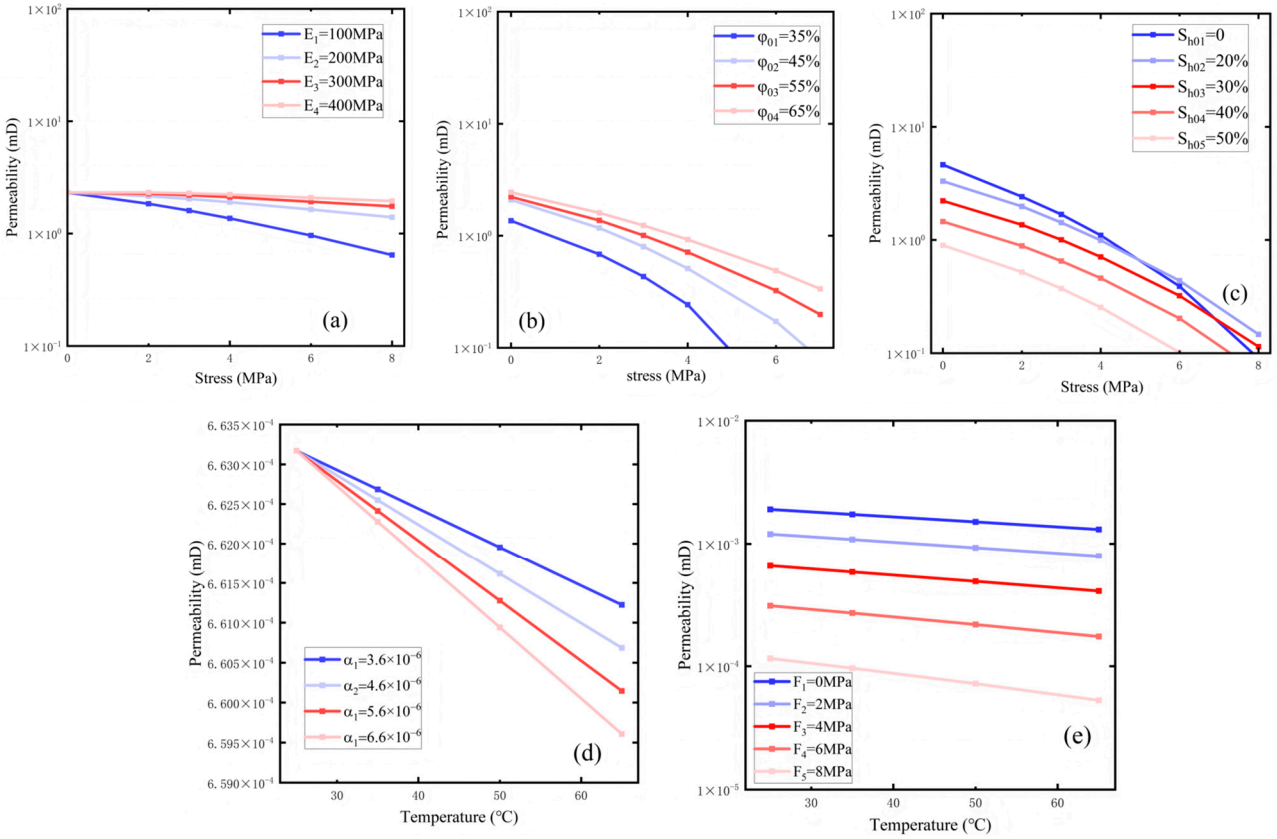


Figure 4. Illustrates the influence of (**a**) elastic modulus, (**b**) initial porosity, (**c**) initial hydrate saturation and stress, (**d**) linear expansion coefficient and temperature, and (**e**) the combined effect of stress and temperature on permeability.

3.3. Model Advantages and Limitations

A fractal theory-based non-empirical model is established in this study to forecast the permeability of natural gas hydrate-bearing sediments. The model's primary advantage lies in its detailed characterization of the heterogeneity inherent in sediment particles and pore structures, which leads to improved prediction accuracy. Furthermore, it systematically integrates the dual mechanisms of effective stress and temperature influence, resulting in a more comprehensive and coherent predictive framework. Notably, the complete absence of empirical parameters endows the model with strong generalization and extrapolation capabilities, allowing for direct application across diverse geological conditions without case-specific parameter adjustments. The model has been validated through experimental data, enhancing its reliability and providing a stronger theoretical basis to guide the efficient development of hydrate sediment resources. Additionally, the influences of different parameters on permeability have been explored through numerical simulations, offering important insights for further understanding the behavior of hydrate sediments.

However, despite these strengths, the derived model also has several drawbacks and is subject to certain assumptions that warrant careful discussion. While the proposed model captures the coupled effects of effective stress, temperature, and particle heterogeneity on permeability, these assumptions may introduce limitations. For instance, simplifying assumptions regarding particle shape and particle spacing may differ from actual conditions and affect the model's accuracy. More specifically, the model assumes elastic deformation of sediment particles following Hooke's law. However, under high effective stress conditions, particle contacts may yield or even fracture, leading to grain crushing and pore collapse. This inelastic behavior is not considered in the current model and may become significant in deep reservoirs or near-wellbore regions. The treatment of particle deformation under increased effective stress in the model may therefore have limitations, as it does not account for potential plastic deformation or other complex deformation processes, potentially leading to inaccuracies in describing certain phenomena.

Additionally, the model assumes that hydrate saturation remains constant during deformation, implying thermodynamic stability of the hydrate phase. This assumption is reasonable for regions far from the production well, where pore pressure exceeds the phase equilibrium pressure. In such regions, hydrate dissociation is negligible, and the model describes the intrinsic permeability evolution of the reservoir. However, in near-wellbore zones with sharp pressure drawdown, hydrate dissociation and its impact on permeability should be considered. Furthermore, temperature affects not only the solid skeleton via thermal expansion but also the fluid viscosity. In practice, an increased temperature reduces fluid viscosity, which may enhance flow and partially offset the permeability reduction caused by pore contraction. The current model focuses on the thermoelastic response of the solid phase; coupling with fluid property changes would provide a more comprehensive assessment of seepage capacity. Consequently, the consideration of particle heterogeneity in the model may still have limitations, failing to fully capture the complexity of real reservoirs.

In summary, the non-empirical fractal model establishes a predictive framework for the permeability of hydrate sediment by considering various influencing factors. However, it requires further refinement and validation to enhance its applicability and accuracy. Future work could incorporate elastoplastic or damage mechanics to address the limitations related to inelastic deformation, as well as consider the effects of hydrate dissociation and fluid property changes to better align the model with reality and improve its prediction accuracy.

4. Conclusions

This paper derives a non-empirical fractal permeability model applicable to sediments containing natural gas hydrates. The model takes into account the influence on permeability brought by effective stress and temperature. By fitting and validating the predicted results with experimental data from previous studies, it demonstrates that the model has good predictive capability for the permeability of sediments containing natural gas hydrates under the consideration of effective stress and temperature. The main conclusions are as follows:

The permeability of hydrate-bearing sediments is governed by a combination of pore structure parameters, hydrate saturation, effective stress, pore fractal dimension, tortuosity fractal dimension, and the heterogeneity parameters θ and m. The model explicitly links these factors through thermoelastic theory and fractal geometry, providing a mechanistic understanding of permeability evolution.

Within the investigated ranges, increases in effective stress and temperature both lead to a reduction in permeability. However, the influence of effective stress is more

pronounced than that of temperature, indicating that mechanical compaction dominates the permeability response under coupled thermo-mechanical conditions.

Hydrates in sediments do not exist in a single mode but rather as a mixture of grain-coating and pore-filling habits. The relative proportions may shift with changing effective stress, as suggested by the model validation. The use of weighting coefficients allows the model to capture such transitions and better represent real reservoir conditions.

Sensitivity analysis reveals that the effective stress, elastic modulus, initial hydrate saturation, and initial porosity have significant impacts on permeability. Temperature and the linear thermal expansion coefficient exert a relatively minor influence, primarily through their effect on pore dilation. These findings highlight the dominant role of mechanical factors in reservoir permeability and provide guidance for EOR strategy design.

Author Contributions: Y.-Y.M.: Conceptualization, Methodology, Validation, Writing—Original Draft. Y.-H.S.: Conceptualization, Methodology, Visualization, Writing—Original Draft. K.-Y.W.: Data Curation, Software, Validation, Writing—Review and Editing. G.L.: Methodology, Funding Acquisition, Resources, Supervision, Writing—Original Draft. All authors have read and agreed to the published version of the manuscript.

Funding: This research was funded by Natural Science Foundation of Hubei Province, China grant number [No. 2025AFB556].

Data Availability Statement: The original contributions presented in this study are included in the article. Further inquiries can be directed to the corresponding author.

Conflicts of Interest: The authors declare no conflicts of interest.

Appendix A. Derivation of Parameter τavF,T

Based on the particle arrangement within a pore unit of HBS [29] shown in Figure A1, with the center-to-center distances b and c, the relationships between porosity φ, particle radius r and m (the ratio of c to b) are as follows:

$$\begin{cases} \varphi = \frac{bc-\pi r^2}{bc} \\ m = \frac{c}{b} \\ \frac{r}{b} = \sqrt{\frac{m(1-\varphi)}{\pi}} \end{cases} \tag{A1}$$

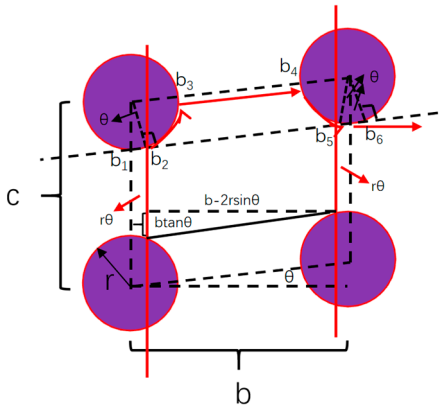


Figure A1. Schematic diagram of the particle arrangement within a pore unit.

Affected by the force F exerted on the particles, based on Hooke's law, the particle radius r_F and the center-to-center distances b_F and c_F are respectively

$$\begin{cases} r_F = r \\ b_F = b\left(1 - \frac{F}{E}\right) \\ c_F = c\left(1 - \frac{F}{E}\right) \end{cases} \tag{A2}$$

According to the theory of linear expansion, the particle radius $r_{F,T}$ and the center-to-center distances $b_{F,T}$ and $c_{F,T}$ are respectively

$$\begin{cases} r_{F,T} = (1 + \alpha\Delta T)r \\ b_{F,T} = b_F = b\left(1 - \frac{F}{E}\right) \\ c_{F,T} = c_F = c\left(1 - \frac{F}{E}\right) \end{cases} \tag{A3}$$

By combining Equations (A1) and (A3), porosity $\varphi_{F,T}$ affected by the effective stress and temperature is

$$\varphi_{F,T} = 1 - \left(\frac{1 + \alpha\Delta T}{1 - \frac{F}{E}}\right)^2 (1 - \varphi_0) \tag{A4}$$

Based on the model of Peng et al. [29], the parameter $\tau_{avF,T}$ is

$$\begin{cases} \tau_1 = \frac{1}{2}\left[\begin{array}{l} \frac{(\pi-2)(1+\alpha\Delta T)r}{b(1-F/E)} + \frac{1}{\cos\theta} \\ + \sqrt{\left(1 - \frac{2(1+\alpha\Delta T)r}{b(1-F/E)}\sin\theta\right)^2 + (\tan\theta)^2} \\ + \frac{2(1+\alpha\Delta T)r\theta}{b(1-F/E)} \end{array}\right] \\ \tau_2 = 1 + \frac{(\pi-2)(1+\alpha\Delta T)r}{2b(1-F/E)} \\ \tau_{avF,T} = \frac{\tau_1+\tau_2}{2} = \left\{\begin{array}{l} \frac{1}{4}\left[\begin{array}{l} \frac{r(\pi-2)(1+\alpha\Delta T)}{b(1-F/E)} + \frac{1}{\cos\theta} + \\ \sqrt{\left(1 - 2\frac{r(1+\alpha\Delta T)}{b(1-F/E)}\sin\theta\right)^2 + (\tan\theta)^2} \\ + \frac{2r\theta(1+\alpha\Delta T)}{b(1-F/E)} \end{array}\right] \\ + \frac{1}{2} + \frac{r(\pi-2)(1+\alpha\Delta T)}{4b(1-F/E)} \end{array}\right\} \end{cases} \tag{A5}$$

References

1. Chong, Z.R.; Yang, S.H.B.; Babu, P.; Linga, P.; Li, X.-S. Review of Natural Gas Hydrates as an Energy Resource: Prospects and Challenges. *Appl. Energy* **2016**, *162*, 1633–1652. [CrossRef]
2. Collett, T.; Bahk, J.-J.; Baker, R.; Boswell, R.; Divins, D.; Frye, M.; Goldberg, D.; Husebø, J.; Koh, C.; Malone, M.; et al. Methane Hydrates in Nature—Current Knowledge and Challenges. *J. Chem. Eng. Data* **2015**, *60*, 319–329. [CrossRef]
3. Makogon, Y.F.; Omelchenko, R.Y. Commercial Gas Production from Messoyakha Deposit in Hydrate Conditions. *J. Nat. Gas Sci. Eng.* **2013**, *11*, 1–6. [CrossRef]
4. Zhang, Z.; Liu, L.; Lu, W.; Liu, C.; Ning, F.; Dai, S. Permeability of Hydrate-Bearing Fine-Grained Sediments: Research Status, Challenges and Perspectives. *Earth Sci. Rev.* **2023**, *244*, 104517. [CrossRef]
5. Walsh, M.R.; Hancock, S.H.; Wilson, S.J.; Patil, S.L.; Moridis, G.J.; Boswell, R.; Collett, T.S.; Koh, C.A.; Sloan, E.D. Preliminary Report on the Commercial Viability of Gas Production from Natural Gas Hydrates. *Energy Econ.* **2009**, *31*, 815–823. [CrossRef]
6. Yang, L.; Liu, Y.; Zhang, H.; Xiao, B.; Guo, X.; Wei, R.; Xu, L.; Sun, L.; Yu, B.; Leng, S.; et al. The Status of Exploitation Techniques of Natural Gas Hydrate. *Chin. J. Chem. Eng.* **2019**, *27*, 2133–2147. [CrossRef]
7. Li, X.-S.; Xu, C.-G.; Zhang, Y.; Ruan, X.-K.; Li, G.; Wang, Y. Investigation into Gas Production from Natural Gas Hydrate: A Review. *Appl. Energy* **2016**, *172*, 286–322. [CrossRef]
8. Jia, C.; Alkaabi, S.; Sepehrnoori, K.; Fan, D.; Yao, J. Numerical Modeling and Studies of the Acid Stimulation Process in Dolomite Carbonate Rocks. *SPE J.* **2023**, *28*, 2165–2185. [CrossRef]
9. Yang, D.; Wang, W.; Chen, W.; Tan, X.; Wang, L. Revisiting the Methods for Gas Permeability Measurement in Tight Porous Medium. *J. Rock Mech. Geotech. Eng.* **2019**, *11*, 263–276. [CrossRef]

10. Yan, C.; Ren, X.; Cheng, Y.; Song, B.; Li, Y.; Tian, W. Geomechanical Issues in the Exploitation of Natural Gas Hydrate. *Gondwana Res.* **2020**, *81*, 403–422. [CrossRef]
11. Ilyushin, Y.V.; Nosova, V.Y. Development of Mathematical Model for Forecasting the Production Rate. Available online: https://www.ije.ir/article_211445.html (accessed on 23 February 2026).
12. Wu, Z.; Yang, S.; Liu, W.; Li, Y. Permeability Analysis of Gas Hydrate-Bearing Sand/Clay Mixed Sediments Using Effective Stress Laws. *J. Nat. Gas Sci. Eng.* **2022**, *97*, 104376. [CrossRef]
13. Li, P.; Zhang, X.; Lu, X.; Liu, L.; Liu, C. Study on Gas Hydrate Dissociation in Small Bodies of Hydrate-Bearing Sediments under Water-Heating Condition. In Proceedings of the ISOPE International Ocean and Polar Engineering Conference, Rhodes, Greece, 26 June–2 July 2016; ISOPE: Mountain View, CA, USA, 2016.
14. Sun, X.; Luo, T.; Wang, L.; Wang, H.; Song, Y.; Li, Y. Numerical Simulation of Gas Recovery from a Low-Permeability Hydrate Reservoir by Depressurization. *Appl. Energy* **2019**, *250*, 7–18. [CrossRef]
15. Gao, Y.; Chen, M. Evaluation of Thermal Stimulation in Hydrate Reservoirs under Hot-Water Cyclic Injection. *Arab. J. Geosci.* **2020**, *13*, 449. [CrossRef]
16. Jesse, F. Comparative Philosophy: Its Aims And Methods. *J. Chin. Philos.* **2003**, *30*, 259–270. Available online: https://onlinelibrary.wiley.com/doi/full/10.1111/1540-6253.00118 (accessed on 6 March 2024).
17. Liu, Y.; Li, Y.; Zhang, Z.; Li, G.; Hou, J.; Ma, C.; Wei, B.; Du, Q.; Zhang, M.; Ji, Y.; et al. Study on Stress Sensitivity of Clayey Silt Hydrate-Bearing Sediments and Its Influence Law on Production. *Water Res.* **2026**, *288*, 124620. [CrossRef] [PubMed]
18. Gong, G.; Zhao, G.; Pang, W.; Yang, M.; Chen, B.; Zheng, J. Review of Hydrate-Bearing Sediment Permeability for Natural Gas Hydrate Exploitation: Measurement and Application Development. *J. Pet. Sci. Eng.* **2023**, *220*, 111217. [CrossRef]
19. Liu, X.; Dong, H.; Yan, W.; Arif, M.; Zhang, Y.; Golsanami, N. Influence of Gas Hydrate Saturation and Pore Habits on Gas Relative Permeability in Gas Hydrate-Bearing Sediments: Theory, Experiment and Case Study. *J. Nat. Gas Sci. Eng.* **2021**, *95*, 104171. [CrossRef]
20. Zhou, S.; Li, Q.; Lv, X.; Fu, Q.; Zhu, J. Key Issues in Development of Offshore Natural Gas Hydrate. *Front. Energy* **2020**, *14*, 433–442. [CrossRef]
21. Bernabe, Y.; Li, M.; Maineult, A. Permeability and Pore Connectivity: A New Model Based on Network Simulations. *J. Geophys. Res.* **2010**, *115*, B10. Available online: https://agupubs.onlinelibrary.wiley.com/doi/full/10.1029/2010JB007444 (accessed on 17 January 2026). [CrossRef]
22. Wang, D.; Ning, F.; Lu, J.; Lu, H.; Kang, D.; Xie, Y.; Li, J.; Sun, J.; Ou, W.; Liu, Z.; et al. Reservoir Characteristics and Critical Influencing Factors on Gas Hydrate Accumulations in the Shenhu Area, South China Sea. *Mar. Pet. Geol.* **2021**, *133*, 105238. [CrossRef]
23. Singh, H.; Javadpour, F.; Ettehadtavakkol, A.; Darabi, H. Nonempirical Apparent Permeability of Shale. *SPE Reserv. Eval. Eng.* **2014**, *17*, 414–424. [CrossRef]
24. Cheng, F.; Wu, Z.; Sun, X.; Shen, S.; Wu, P.; Liu, W.; Chen, B.; Liu, X.; Li, Y. Compression-Induced Dynamic Change in Effective Permeability of Hydrate-Bearing Sediments during Hydrate Dissociation by Depressurization. *Energy* **2023**, *264*, 126137. [CrossRef]
25. Sun, Y.Z.; Xie, L.Z.; He, B.; Gao, C.; Wang, J. Effects of Effective Stress and Temperature on Permeability of Sandstone from CO_2 -Plume Geothermal Reservoir. *J. Rock Mech. Geotech. Eng.* **2016**, *8*, 819–827. [CrossRef]
26. Song, Y.; Zhu, Y.; Liu, W.; Li, Y.; Lu, Y.; Shen, Z. The Effects of Methane Hydrate Dissociation at Different Temperatures on the Stability of Porous Sediments. *J. Pet. Sci. Eng.* **2016**, *147*, 77–86. [CrossRef]
27. Shang, Y.-H.; Lei, G.; Yuan, X.-Y.; Wang, K.-Y.; Qiu, K.-X. Development of an Innovative Permeability Model for Hydrate-Bearing Sediments under Creep Conditions: Effects of Particle Shape and Non-Uniform Particle Distribution. *Pet. Sci.* **2025**, *23*, 524–540. [CrossRef]
28. Guo, Z.; Fang, Q.; Nong, M.; Ren, X. A Novel Kozeny-Carman-Based Permeability Model for Hydrate-Bearing Sediments. *Energy* **2021**, *234*, 121203. [CrossRef]
29. Peng, H.; Li, X.; Chen, Z.; Zhang, Y.; Ji, H.; You, C. Permeability Properties of Hydrate-Bearing Sediments: Competition and Conversion in Hydrates Growth. *Gas Sci. Eng.* **2023**, *118*, 205089. [CrossRef]
30. Tang, J.; Lei, G.; Li, X.; Zhang, L.; Cheng, W.; Pang, J.; Jiang, G. A novel analytical model of the effective thermal conductivity of porous materials under stress. *Fractals* **2023**, *31*, 2340176. [CrossRef]
31. Lei, G.; Gong, Z.; He, Z.; Wu, Q.; Guan, J.; Zhang, L. Theoretical Analysis of Shape Factor of Gas Hydrate Sediments under Stress Dependence. *Gas Sci. Eng.* **2023**, *119*, 205137. [CrossRef]
32. Kleinberg, R.L.; Flaum, C.; Griffin, D.D.; Brewer, P.G.; Malby, G.E.; Peltzer, E.T.; Yesinowski, J.P. Deep Sea NMR: Methane Hydrate Growth Habit in Porous Media and Its Relationship to Hydraulic Permeability, Deposit Accumulation, and Submarine Slope Stability. *J. Geophys. Res. Solid Earth* **2003**, *108*, B10. Available online: https://agupubs.onlinelibrary.wiley.com/doi/full/10.1029/2003JB002389 (accessed on 3 February 2026). [CrossRef]

33. Du, P.; Zhao, C.; Peng, P.; Gao, T.; Huang, T. Fractal Characterization of Permeability Prediction Model in Hydrate-Bearing Porous Media. *Chem. Eng. Sci.* **2020**, *218*, 115576. [CrossRef]
34. Yu, B.; Cheng, P. A Fractal Permeability Model for Bi-Dispersed Porous Media. *Int. J. Heat Mass Transf.* **2002**, *45*, 2983–2993. [CrossRef]
35. Zhang, Z.; Liu, L.; Ning, F.; Liu, Z.; Sun, J.; Li, X.; Sun, J.; Hyodo, M.; Liu, C. Effect of Stress on Permeability of Clay Silty Cores Recovered from the Shenhu Hydrate Area of the South China Sea. *J. Nat. Gas Sci. Eng.* **2022**, *99*, 104421. [CrossRef]

Disclaimer/Publisher's Note: The statements, opinions and data contained in all publications are solely those of the individual author(s) and contributor(s) and not of MDPI and/or the editor(s). MDPI and/or the editor(s) disclaim responsibility for any injury to people or property resulting from any ideas, methods, instructions or products referred to in the content.